State-to-State Vibrational Energy Transfer in OH $A^2\Sigma^+$ with N_2

Timothy D. Sechler, Logan P. Dempsey, and Marsha I. Lester*

Department of Chemistry, University of Pennsylvania, Philadelphia, Pennsylvania 19104-6323

Received: May 27, 2009; Revised Manuscript Received: June 18, 2009

Vibrational energy transfer from $v' = 0$ to $v' = 1$ in the excited OH $A^2\Sigma^+$ electronic state is investigated in the collisional region of a free-jet expansion. Laser excitation is used to prepare high rotational levels in OH $A^2\Sigma^+$ ($v' = 0$, $N' = 14-22$), which lie above the energetic threshold for OH $A^2\Sigma^+$ ($v' = 1$). Subsequent collisions with N_2 result in population of a distribution of OH $A^2\Sigma^+$ ($v' = 1$) product rotational levels that is characterized through dispersed fluorescence spectra. The majority of products are found in the most near-resonant rotational level of $v' = 1$, with population falling off exponentially in lower rotational levels. Additionally, the efficiency of vibrational energy transfer is determined by comparing the emission from $v' = 1$ products with that from the initially prepared $v' = 0$ level. The fractional transfer decreases by an order of magnitude from the highest to lowest initial rotational levels investigated. This decrease is correlated with an increasingly large change in rotational angular momentum between the initial and final states. The results show that angular momentum constraints are the dominant factor in the efficiency of OH $A^2\Sigma^+$ $v' = 0$ to $v' = 1$ vibrational energy transfer at low collision energies.

I. Introduction

The hydroxyl radical plays a central role in atmospheric and combustion environments, where it is often detected via laser induced fluorescence (LIF) on the $A^2\Sigma^+-X^2\Pi$ transition. However, collisions with molecular partners that can redistribute OH $A^2\Sigma^+$ population are common in these environments. It is important to characterize the rates and outcomes of these processes to account for their effects on measurement of ground-state populations. Specifically, collisional quenching results in the nonradiative removal of population from the $A^2\Sigma^+$ state, either through reaction or transfer back to the ground $X^2\Pi$ state, which reduces the fluorescence quantum yield. In addition, collisions with molecular partners can induce the transfer of population to other rovibrational levels within the excited OH $A^2\Sigma^+$ electronic state. The studies presented here examine state-to-state vibrational energy transfer (VET) within the OH $A^2\Sigma^+$ electronic state upon collision with N_2.

Quenching of OH $A^2\Sigma^+$ by collisions with N_2 has been characterized previously by kinetic studies.[1−7] These studies revealed that the quenching cross section exhibits a negative temperature dependence, indicating that attractive forces are important.[1,2,4,6] Furthermore, the cross section decreases with initial OH $A^2\Sigma^+$ rotational excitation, suggesting that specific orientations of the collision pair are required for quenching.[3,5,7,8] Quenching of OH $A^2\Sigma^+$ by N_2 has two possible outcomes: reactive quenching producing $N_2O + H$ ($\Delta E = -1.03$ eV) and nonreactive quenching resulting in OH $X^2\Pi + N_2$ ($\Delta E = -4.02$ eV).

Recent collisional quenching studies conducted in this laboratory have focused on measuring the quantum state distribution of OH $X^2\Pi$ products and the branching fraction for the nonreactive pathway.[8] These studies revealed that OH $X^2\Pi$ products are generated with little vibrational excitation, mostly in $v'' = 0$, but with substantial rotational excitation. The OH $X^2\Pi$ ($v'' = 0$) product state distribution peaks at $N'' = 18$ with an average rotational energy of $\sim$6500 cm^{-1}. Branching fraction measurements revealed that nonreactive quenching accounts for $\geq$88% of the total quenched products. The balance is most likely OH $X^2\Pi$ products in very high rotational levels of $v'' = 0$ that could not be probed due to experimental limitations.

Complementary theoretical studies have shown that collisional quenching of OH $A^2\Sigma^+$ by N_2 occurs through regions of conical intersection (CI) that couple the electronic ground $X^2\Pi$ and excited $A^2\Sigma^+$ state surfaces when the oxygen side of OH points toward N_2.[8,9] Recent work has examined the topography of the potential energy surfaces in the vicinity of the CI. These calculations revealed that a large torque is placed on the OH moiety as it passes through the CI, generating substantial rotational excitation of OH $X^2\Pi$ products. The calculations further show a significant tilt of the cone strongly favoring the nonreactive quenching pathway. The rotational distribution of OH $X^2\Pi$ products and branching fraction observed experimentally are thus shown to be dynamical signatures of nonadiabatic passage through the CI region.

For OH $A^2\Sigma^+ + N_2$, other collision induced processes, including rotational energy transfer (RET) and VET, can occur with comparable efficiency as quenching.[6,7,10−13] For example, at room temperature the rate coefficient for VET is 10 times larger than that for quenching.[7] RET studies within OH $A^2\Sigma^+$ ($v' = 0$, 1) have shown that the rate of transfer between rotational levels decreases with increasing change in the number of rotational quanta (ΔN) transferred and the magnitude of the energy gap between the initial and final levels. These kinetic trends were found to be similar for the OH $A^2\Sigma^+$ $v' = 0$ and 1 vibrational states.[11,12]

Vibrational energy transfer within the OH $A^2\Sigma^+$ state induced by collisions with N_2 has been examined previously.[7,10,13−15] These studies focused primarily on transfer from $v' = 1$ to $v' = 0$, where the rate of transfer increases as the temperature is lowered from 297 to 196 K and decreases with increasing initial rotational excitation in $v' = 1$. Interestingly, a broad product rotational distribution was observed in $v' = 0$, and the shape of

* To whom correspondence should be addressed. Tel.: (215) 898-4640. Fax: (215) 573-2112. E-mail: milester@sas.upenn.edu.

10.1021/jp904978w CCC: $40.75
Published on Web 07/15/2009

the distribution did not depend markedly on the initial N' level prepared in $v' = 1$.[7,15,16]

In addition, vibrational energy transfer from $v' = 0$ to $v' = 1$ has been observed at flame temperatures (~1400 K).[14] These studies focused on specific initial states of OH $A^2\Sigma^+$ ($v' = 0$, $N' = 4$, 9, and 14), where dispersed fluorescence measurements showed that similar fractional populations were transferred to $v' = 1$. However, these experiments did not measure the rotational distribution of the OH $A^2\Sigma^+$ ($v' = 1$, N') products.

In this paper, we investigate vibrational energy transfer in OH $A^2\Sigma^+$ from $v' = 0$ to $v' = 1$ by N_2 at low collision energies in the collisional region of a free jet expansion. We determine the rotational distribution of OH $A^2\Sigma^+$ ($v' = 1$, N') products and find that a near-resonant product rotational level is dominant. In addition, we examine the relative efficiency of population transfer as a function of the initial OH $A^2\Sigma^+$ ($v' = 0$, N') rotational level. We deduce that angular momentum constraints control the efficiency of the collisional energy transfer process.

II. Experimental Methods

Hydroxyl radicals are generated by 193 nm (ArF Excimer, Lambda Physik Compex 102) photolysis of a nitric acid precursor entrained in a 20% N_2 in He carrier gas (150 psi) near the exit of a solenoid pulsed valve (General Valve Series 9). At approximately $x/D = 5$ nozzle diameters downstream in the collisional region of the supersonic expansion, a UV pump laser beam, generated by frequency doubling the output of a Nd:YAG pumped dye laser (Continuum Surelite II with TDL60), crosses the gas pulse. The rotational temperature of OH $X^2\Pi$ at this location is ~50 K, which we take as an estimate of the translational temperature. The pump laser beam excites OH radicals on the $P_1(1)$ line of the OH A-X (0,0) transition at 308 nm. Following a 200 ns delay, which allows for collisional quenching of OH $A^2\Sigma^+$ ($v' = 0$, $N' = 0$) by N_2, a second spatially overlapped and counterpropagating UV laser beam is introduced. This laser excites rotationally excited OH $X^2\Pi$ ($v'' = 0$) products of quenching as well as any residual OH $X^2\Pi$ present in these levels from photolysis of HNO_3 on the A-X (0,0) transition at 310 nm. The UV radiation for this second excitation step is generated by frequency doubling the output of a Nd:YAG (Innolas, SL600) pumped dye laser (Radiant Dyes, Narrowscan). The second step prepares OH in high rotational levels of $A^2\Sigma^+$ ($v' = 0$, N') that can be transferred by collision with N_2 to OH $A^2\Sigma^+$ ($v' = 1$).

Two types of experiments are carried out: dispersed fluorescence and population transfer measurements. Dispersed fluorescence measurements are performed to obtain the rotational distribution of the OH $A^2\Sigma^+$ ($v' = 1$, N') products from VET. For these measurements, fluorescence is collected using an *f*/1 (f ≈ 0.05 m) lens to collimate and a second *f*/6 (f ≈ 0.30 m) lens is used to focus the fluorescence onto the entrance slit (0.25 mm width) of a 0.3 m scanning monochromator (McPherson), resulting in 6.5 Å resolution. The dispersed fluorescence is detected with a photomultipier tube (PMT) mounted on the exit slit of the monochromator. The signal from the PMT is monitored using a digital oscilloscope interfaced with a PC and integrated over a 1 μs gate.

The second type of experiment measures the efficiency of population transfer from the initially prepared OH $A^2\Sigma^+$ ($v' = 0$, N') level to OH $A^2\Sigma^+$ ($v' = 1$). This is achieved by comparing the intensity of emission from $v' = 0$ with that from $v' = 1$ by selectively collecting the fluorescence from each vibrational state using bandpass filters. Emission from OH $A^2\Sigma^+$ ($v' = 1$) is collected on the A-X (1,0) band using a bandpass filter centered at 280 ± 12.5 nm in combination with a 325 nm mirror to block the intense fluorescence induced by the pump laser beam; emission from $v' = 0$ is collected on the A-X (0,0) band using a 323 ± 5 nm bandpass filter with a 315 nm long-pass filter. In this case, the fluorescence is integrated with a 5 μs gate.

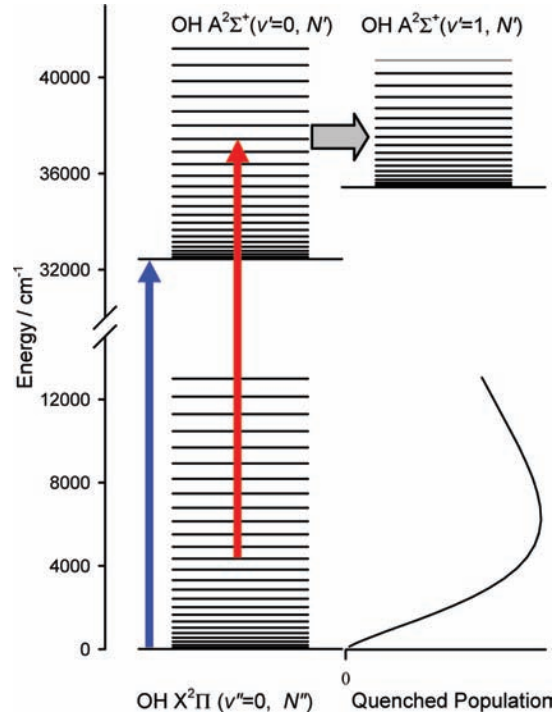

Figure 1. Schematic energy level diagram depicting two step laser excitation scheme, quenched population distribution and vibrational energy transfer (VET) process within the OH $A^2\Sigma^+$ state. The pump laser (blue arrow) prepares OH in the lowest rovibrational level of the $A^2\Sigma^+$ state. The OH $A^2\Sigma^+$ ($v' = 0$, $N' = 0$) state is collisionally quenched by N_2 to give the highly rotationally excited $X^2\Pi$ population distribution shown (bottom right). After a 200 ns delay, the second laser (red arrow) prepares high rotational levels ($N' = 14-22$) in OH $A^2\Sigma^+$ ($v' = 0$) that lie above the energetic threshold for $v' = 1$. Subsequent collisions induce VET from $v' = 0$ to 1. The fluorescence from OH $A^2\Sigma^+$ ($v' = 1$) is dispersed to characterize the rotational states populated by VET.

III. Results and Analysis

High rotational levels of OH in its excited $A^2\Sigma^+$ ($v' = 0$) electronic state, which are the starting point for the state-to-state VET studies presented here, are populated by a multistep process illustrated in Figure 1: A pump laser initially prepares OH $A^2\Sigma^+$ ($v' = 0$, $N' = 0$), which is quenched by collision with N_2, producing highly rotationally excited levels of OH in its ground $X^2\Pi$ ($v'' = 0$) electronic state. The OH $X^2\Pi$ ($v'' = 0$) quantum state distribution has been previously characterized under single collision conditions,[8] as summarized in the Introduction, and is shown for reference in Figure 1. OH $X^2\Pi$ ($v'' = 0$) population in high rotational levels is then excited with a second UV laser to prepare OH in specific rotational levels ($N' = 14-22$) of the excited $A^2\Sigma^+$ ($v' = 0$) state, which lie above the energetic threshold for OH $A^2\Sigma^+$ ($v' = 1$). Subsequent collisions with N_2 transfer population from a specific ($v' = 0$, N') level to $v' = 1$ within the excited OH $A^2\Sigma^+$ electronic state.

A. Dispersed Fluorescence Measurements. Prior to examining the OH $A^2\Sigma^+$ ($v' = 1$) products of VET, the fluorescence from the initially prepared OH $A^2\Sigma^+$ ($v' = 0$) state is dispersed. These dispersed fluorescence spectra show that the emission

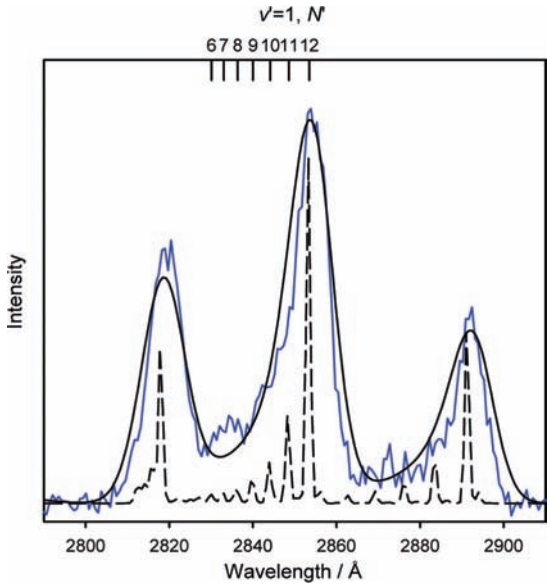

Figure 2. The dispersed fluorescence spectrum (blue) of emission from OH $A^2\Sigma^+$ $v' = 1$ induced by collisions with N_2 following laser excitation to OH $A^2\Sigma^+$ ($v' = 0$, $N' = 18$). Partially resolved rotational structure associated with emission on main branch P, Q, and R lines is observed. The simulation (solid line, 6.5 Å resolution) shows that the majority of the fluorescence originates from $v' = 1$, $N' = 12$. A best fit was obtained using an energy gap relationship (see text), giving rise to an exponential tail falling off to lower rotational levels. The contribution from lower rotational levels is seen more clearly in a higher resolution simulation (1.0 Å) that displays the individual rotational levels (dashed line).

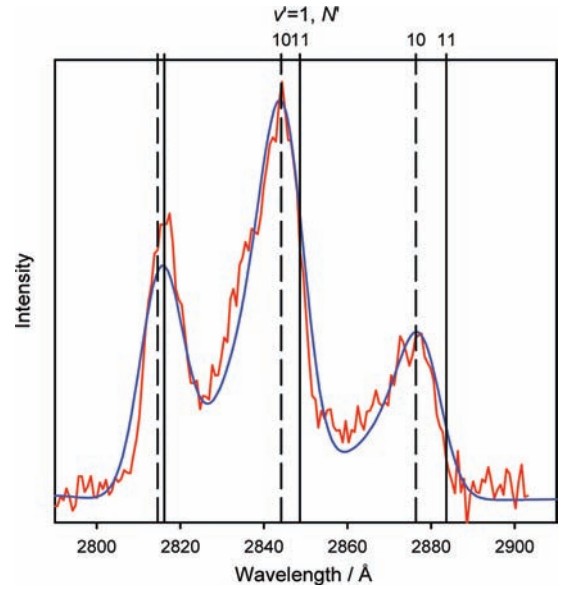

Figure 3. The dispersed fluorescence spectrum (red) from OH $A^2\Sigma^+$ $v' = 1$ following excitation to $A^2\Sigma^+$ ($v' = 0$ $N' = 17$). Simulation of this emission shows that the majority of the emission originates from $N' = 10$ (P, Q and R main branch line positions are indicated by dashed vertical lines). There was no discernible contribution from OH $A^2\Sigma^+$ ($v' = 1$, $N' = 11$), the most near resonant rotational level (line positions indicated by solid vertical lines).

originates from the initially prepared rotational level with no significant energy transfer to other rotational levels in OH $A^2\Sigma^+$ ($v' = 0$). On the other hand, despite preparation of a single spin-rotation state (typically F_1), emission is observed from both spin-rotation states with the same N'. This suggests that spin-rotation transfer is more efficient than rotational energy transfer for the high rotational levels of OH $A^2\Sigma^+$ ($v' = 0$) investigated under the present experimental conditions.[17] Additionally, the dispersed fluorescence spectra from the OH $A^2\Sigma^+$ ($v' = 1$) products of VET (see below) is unchanged with the spin-rotation state (F_1 or F_2) selected in the initially prepared OH $A^2\Sigma^+$ ($v' = 0$, N') level.

Dispersed fluorescence spectra originating from the OH $A^2\Sigma^+$ ($v' = 1$) products of VET are recorded on the A-X (1,0) band for each of the initially prepared OH $A^2\Sigma^+$ ($v' = 0$, $N' = 14-22$) levels. Representative dispersed fluorescence spectra are shown as a function of wavelength (λ, Å) in Figures 2 and 3 for the initially prepared $N' = 18$ and 17 levels, respectively. Partially resolved rotational structure associated with emission on main branch P, Q, and R lines is observed. Spectral analysis, detailed below, shows that the emission originates principally from a single near-resonant OH $A^2\Sigma^+$ ($v' = 1$, N') rotational level. The asymmetry of the main branch lines, however, indicates that there are also smaller contributions to the emission profile from several product rotational levels.

Emission is observed only from OH $A^2\Sigma^+$ ($v' = 1$, N') product rotational levels that lie lower in energy than the initially prepared level in $v' = 0$, namely, $E_i \geq E_N$. The absence of upward transitions to product rotational levels with $E_N \geq E_i$ is not surprising, given the low collision energy in the supersonic jet. The latter point is illustrated in Figure 3, where the dispersed fluorescence from OH $A^2\Sigma^+$ ($v' = 1$, N') is shown following excitation of OH $A^2\Sigma^+$ ($v' = 0$, $N' = 17$). In this case, a near-resonant upward transition to $v' = 1$, $N' = 11$ ($\Delta E = -80$ cm^{-1}) is not observed; rather, the dominant product channel is $N' = 10$ ($\Delta E = +265$ cm^{-1}). As illustrated in Figure 3, the spacings between the main branch lines enable the dominant final state to be readily determined even with the moderate monochromator resolution available in the present experiments.

Rotational distributions of the OH $A^2\Sigma^+$ ($v' = 1$, N') products of VET are then derived from dispersed fluorescence spectra obtained for each initially prepared level. This is achieved through an iterative procedure in which the product rotational distribution is varied, the corresponding dispersed fluorescence spectrum is simulated, and the simulation is compared with the observed emission spectrum until satisfactory agreement is achieved.

The rotational distribution of the OH $A^2\Sigma^+$ ($v' = 1$) products is assumed to follow an energy gap relationship,[18] in which the population falls off exponentially with increasing energy spacing $\Delta E \equiv E_i - E_N$ between the initial and final states. Term energies are taken from ref 19. The distribution is characterized with a single adjustable fitting parameter β. The normalized population in a given product rotational state N is given by

$$P_N = C \exp\left(\frac{-\sqrt{\Delta E}}{\beta}\right)$$

where C is a normalization constant. Both spin-rotation states of each OH $A^2\Sigma^+$ ($v' = 1$, N') level are included, which results in nearly equal population of the two spin-rotation states for a given N'.

The dispersed fluorescence spectra are simulated using a Gaussian instrument function with monochromator resolution w to represent the line shape and summing over the A-X (1,0) emission lines (denoted with index j) originating from each OH ($v' = 1$, N') product rotational state

$$\sum_N \sum_j P_N Y_N \left(A_{N,j} \exp\left(\frac{\lambda - \lambda_{N,j}}{w} \right)^2 \right)$$

A second sum is carried out over populated product rotational levels. Here, N denotes the rotational level in $v' = 1$ from which emission originates and P_N is the population of that level. $A_{N,j}$ is the emission coefficient and $\lambda_{N,j}$ is the line position for the transition. In general, for each rovibrational level in the OH $A^2\Sigma^+$ state, there are twelve emission lines associated with each A−X vibronic transition. The emission coefficients and line positions are obtained from the LIFBase compilation.[20] The quantum yield Y_N for each OH $A^2\Sigma^+$ ($v' = 1$, N') product state is determined from the fluorescence lifetime measured under the present experimental conditions and the known radiative lifetime.[20]

The best fits of the dispersed fluorescence spectra yielded β parameters ranging from 8−11 $cm^{-1/2}$ that characterize the OH $A^2\Sigma^+$ ($v' = 1$, N') product rotational distribution; the β parameters are tabulated in Table 1. These values for β indicate that the majority of OH $A^2\Sigma^+$ ($v' = 1$) products of VET are found in the near-resonant level (listed in Table 1) lying below the initial state, with the population falling off rapidly in lower rotational levels. The highest populated OH $A^2\Sigma^+$ ($v' = 1$, N') product levels are most favored energetically, that is, minimum energy gap, but involve a substantial change in rotational quantum number with ΔN of 5−9. Typical product rotational distributions are also illustrated as bar graphs in Figure 4 for several of the initially prepared levels.

B. Population Transfer Measurements. The efficiency of VET from an initially prepared OH $A^2\Sigma^+$ ($v' = 0$, N') level to OH $A^2\Sigma^+$ ($v' = 1$) products is determined by comparing the intensity of fluorescence from $v' = 0$ and $v' = 1$ using bandpass filters. The OH $A^2\Sigma^+$ ($v' = 0$) emission occurs from the initially prepared rotational level, N'. The emission from OH $A^2\Sigma^+$ ($v' = 1$) originates from a distribution of product rotational levels determined in dispersed fluorescence measurements. For OH $A^2\Sigma^+$ ($v' = 0$ and 1) emission, both spin-rotation states associated with each rotational level are populated.

Measured fluorescence intensities $I(v)$ from OH $A^2\Sigma^+$ ($v' = 0$ or 1) are related to the corresponding excited state populations $P(v)$ using an analysis procedure that takes into account the fluorescence quantum yield (Y_N) and emission coefficient ($A_{N,j}$) of the emitting v', N' level, and the transmission efficiency (T_N) of the spectral filters used.

$$P(v) \sim \frac{I(v)}{\sum_N P_N T_N Y_N}$$

Here, P_N is the normalized population in a given rotational state N, which is derived from dispersed fluorescence measurements. The sum runs over all populated rotational levels in a given vibrational state. The fraction of emission transmitted through the spectral filters T_N is given by

$$T_N = \frac{\sum_j T_{N,j}(\lambda_{N,j}) A_{N,j}}{\sum_j A_{N,j}}$$

where the summation index j spans over the allowed transitions from the upper state. Other parameters are defined in the previous section.

TABLE 1: Relative Population Transferred to OH $A^2\Sigma^+$ ($v' = 1$) upon Collision With N_2 from Selectively Prepared Initial OH $A^2\Sigma^+$ ($v' = 0$, N') Levels[a]

OH $A^2\Sigma^+$ ($v' = 0$, N')	$P(v' = 1)/P(v' = 0)$, %	β, $cm^{-1/2}$	OH $A^2\Sigma^+$ ($v' = 1$, N')	ΔN
14	0.5(1)	10	5	9
15	1.4(1)	11	7	8
16	1.9(1)	11	9	7
17	1.5(2)	8	10	7
18	2.1(3)	9	12	6
19	1.5(2)	9	13	6
20	3.7(8)	11	15	5
21	5.4(14)	8	16	5
22	5.7(15)	8	17	5

[a] The dominant OH $A^2\Sigma^+$ ($v' = 1$, N') product rotational level and the corresponding change in rotational quantum number (ΔN) are listed along with the fitting parameter β used to characterize the product rotational distribution (see text).

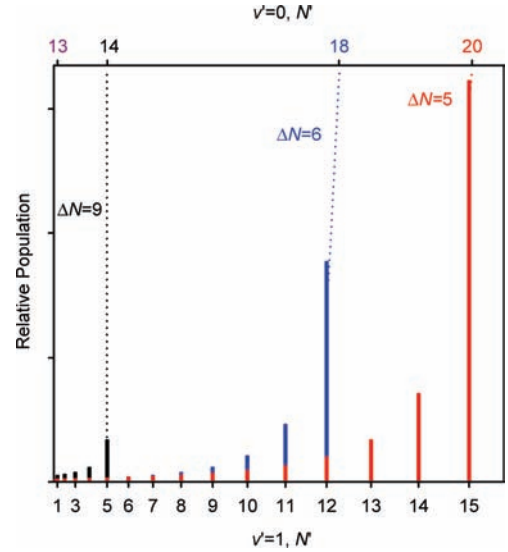

Figure 4. OH $A^2\Sigma^+$ ($v' = 1$, N') population distributions extracted from simulations of dispersed fluorescence spectra. The initially prepared OH $A^2\Sigma^+$ ($v' = 0$, N') level is indicated on the upper axis. The OH $A^2\Sigma^+$ ($v' = 1$, N') product state distributions resulting from excitation to $v' = 0$, $N' = 20$ (red), $N' = 18$ (blue) and $N' = 14$ (black) are displayed as a function of term energy. The relative population transferred from $v' = 0$, N' to $v' = 1$ for each N' is measured separately and used to scale the $v' = 1$, N' relative population distributions.

The fractional population transferred from $v' = 0$ to $v' = 1$, $P(v' = 1)/P(v' = 0)$, for specific initial OH $A^2\Sigma^+$ ($v' = 0$, $N' = 14-22$) levels is listed in Table 1. The results indicate that ~5% of the initial OH $A^2\Sigma^+$ ($v' = 0$, $N' = 22$) population is transferred to $v' = 1$ by collisions with N_2 under the present experimental conditions. The fraction transferred to $v' = 1$ decreases for lower initial rotational levels, dropping to ~0.5% (an order of magnitude smaller) when starting from OH $A^2\Sigma^+$ ($v' = 0$, $N' = 14$). The corresponding change in rotational quantum number for the dominant OH $A^2\Sigma^+$ ($v' = 0$, N') product rotational level (see Table 1) increases significantly from $\Delta N = 5$ to 9 over this range of initial states. No emission is observed from $v' = 1$ following preparation of the next lower initial level, OH $A^2\Sigma^+$ ($v' = 0$, $N' = 13$), indicating no measurable VET occurs. This is unexpected because a near-resonant product state, OH $A^2\Sigma^+$ ($v' = 1$, $N' = 1$), is energetically accessible at slightly lower energy ($\Delta E = +0.5$ cm^{-1}), but involves an even larger change in rotational quantum number of $\Delta N = 12$. Population transfer from yet higher initial rotational levels of OH $A^2\Sigma^+$ ($v' = 0$, $N' \geq 23$) could not be examined due to the onset of

electronic predissociation in OH $A^2\Sigma^+$ ($v' = 0$) as well as extensive predissociation of product states in $v' = 1$. The latter is so rapid as to preclude detection of fluorescence emission from near-resonant OH $A^2\Sigma^+$ ($v' = 1$, $N' \geq 18$) product states.

The relative efficiency of vibrational energy transfer from different initial OH $A^2\Sigma^+$ ($v' = 0$) states is illustrated in Figure 4. Here, the product rotational distributions in $v' = 1$ obtained from dispersed fluorescence measurements are summed and scaled to reflect the relative population transferred from $v' = 0$ (Table 1). Selected initial states in OH $A^2\Sigma^+$ ($v' = 0$) and the corresponding product rotational distributions in $v' = 1$ are plotted in Figure 4. Again, it can be seen that VET is most efficient for higher initial OH $A^2\Sigma^+$ ($v' = 0$, N') levels with smaller changes in rotational quantum number. In addition, population is transferred principally to the near resonant rotational level in OH $A^2\Sigma^+$ ($v' = 1$) that lies lower in energy than the initial state.

IV. Discussion

The experimental observations of state-to-state VET in OH $A^2\Sigma^+$ from $v' = 0$ to 1, namely efficiency of transfer and product state distribution, are discussed in terms of the energy transfer model developed by McCaffery and co-workers.[21−26] In this model for inelastic energy transfer, the change in rotational angular momentum results from conversion of linear to angular momentum at the repulsive wall of the intermolecular potential. The magnitude of ΔN is constrained by conservation of energy and angular momentum. Taking N_2 to be a structureless collision partner, the change in angular momentum of OH upon VET is balanced by the associated change in orbital angular momentum of the OH−N_2 collision pair

$$\Delta N = \mu v_{rel} b$$

Here, μ is the reduced mass of the OH−N_2 collision pair, v_{rel} is the relative velocity of the collision pair, and b is the effective impact parameter or torque arm. The plot of ΔN as a function of v_{rel} for a given b is called an A-plot. The initial distribution of relative collision velocities is simulated as a Maxwell−Boltzmann distribution at 50 K under the present experimental conditions and indicated by the shaded area in Figure 5.

The maximum impact parameter, b_{max}, corresponds to the distance from the center-of-mass to either end of the molecule. Previous studies carried out by McCaffery and co-workers determined values of $b_{max} = 0.13$ and 0.88 Å for OH,[24] corresponding to the distance to the oxygen and hydrogen ends of the molecule, respectively. The A-plot in Figure 5 is based on $b_{max} = 0.88$ Å, in which the collision occurs on the H end of OH. In general, there is a distribution of torque-arm lengths which are sampled up to b_{max}; values less than b_{max} will require even larger v_{rel} for a given ΔN.

The difference in energy between the initial and final states of OH, ΔE, is balanced by the change in kinetic energy of the OH−N_2 collision pair. The energy balance is represented by the E-plot as the change in relative velocity required for each product state.

$$\Delta E = \frac{1}{2}\mu v_{rel}^2$$

E-plots for selected initial OH $A^2\Sigma^+$ ($v' = 0$, N') levels, specifically $N' = 13$, 14, 18, and 20, are shown in Figure 5.

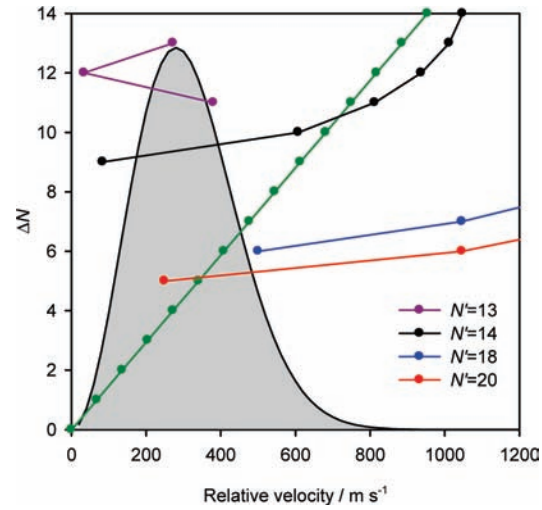

Figure 5. McCaffery model for collision-induced energy transfer for OH $A^2\Sigma^+$ from selected initial $v' = 0$, N' levels to $v' = 1$ by N_2. The A-plot (green) with a torque arm of 0.88 Å indicates the relative collision velocity required for a given change in rotational quantum number (ΔN). The E-plots for selected initial rotational levels, $N' = 20$ (red), $N' = 18$ (blue), $N' = 14$ (black), and $N' = 13$ (purple), give the relative velocity needed for energy balance between the initial and final states. Also shown is a Maxwell−Boltzmann distribution at 50 K (shaded gray region) representing the initial velocity distribution under the present experimental conditions.

The initial relative velocity distribution severely limits the availability of endoergic product channels; only one such process is shown for OH $A^2\Sigma^+$ ($v' = 0$, $N' = 13$) with $\Delta N = 11$.

The upward arching E-plots shown in Figure 5 indicate the change in relative velocities required for satisfying energy balance in these exoergic processes. For a given initial state, the E-plot maps the change in v_{rel} associated with each ΔN; the most near-resonant channel results in the smallest change in ΔE and v_{rel}, and is therefore most favorable on energetic grounds. As the initial rotational level in OH $A^2\Sigma^+$ ($v' = 0$, N') is decreased, an equal or larger ΔN is generally required for transfer to the most near resonant channel in $v' = 1$ (see Table 1).

The change in relative velocity needed to satisfy the angular momentum constraint increases linearly with the magnitude of ΔN. This constraint becomes increasingly difficult to satisfy for larger ΔN transitions and, in some cases, can prevent population transfer. For example, collisional transfer from OH $A^2\Sigma^+$ ($v' = 0$, $N' = 13$) to OH $A^2\Sigma^+$ ($v' = 1$, $N' = 1$) by N_2 is near-resonant as shown in the E-plot, but the transition between the two states requires $\Delta N = 12$. The relative velocity required for orbital angular momentum to balance this large ΔN change (A-plot) is not satisfied. As a result, the angular momentum constraint precludes energy transfer, consistent with the lack of emission observed from $v' = 1$ following preparation of OH $A^2\Sigma^+$ ($v' = 0$, $N' = 13$).

The E-plots shown in Figure 5 for initial OH $A^2\Sigma^+$ ($v' = 0$, $N' = 14$, 18, 20) similarly indicate a near-resonant product rotational channel requiring only a small change in ΔE or relative velocity. On the other hand, these near-resonant transitions still require substantial change in ΔN. A significant change in relative velocity is needed to balance the change in rotational angular momentum, making angular momentum the dominant constraint in the VET process. The ΔN required for the near-resonant product channel decreases with increasing initial OH $A^2\Sigma^+$ ($v' = 0$, N') level from $\Delta N = 9$ for $N' = 14$ to $\Delta N = 6$ for $N' = 18$, and further decreases $\Delta N = 5$

for $N' = 20$. This suggests that the angular momentum constraint would be relaxed with increasing initial OH $A^2\Sigma^+$ ($v' = 0$, N') level, leading to more efficient VET for higher initial N' levels. This trend is observed experimentally, where we find a larger percentage of population transferred to $v' = 1$ for higher initial rotational levels of OH $A^2\Sigma^+$ ($v' = 0$) with $N' = 20 > N' = 18 > N' = 14$ (see Table 1 and Figure 4) at low collision energies. We note that prior studies of VET starting from lower initial rotational levels of OH $A^2\Sigma^+$ ($v' = 0$) at flame temperature did not reveal this trend.[14] In this case, the angular momentum constraint is satisfied due to the much higher initial velocities.

The full McCaffery model[26] was used to predict the probability of state-to-state energy transfer for specific initial OH $A^2\Sigma^+$ ($v' = 0$, N') states and the resultant OH $A^2\Sigma^+$ ($v' = 1$) product rotational distributions. The full treatment (see eq 13 of ref 26) takes into account the distribution of initial velocities of the collision partners and integrates over the range of impact parameters (with an assumed inverse exponential functional form). The overall probability of VET transfer from a given initial state is obtained by summing over the product rotational distribution. The model predicts that the probability of VET changes by an order of magnitude over the range of initial OH $A^2\Sigma^+$ ($v' = 0$, N') states investigated experimentally ($N' = 14-22$), with the probability of transfer largest for high initial N'. Thus, the model captures the trend observed experimentally (Table 1). The product state distributions predicted from the McCaffery model are strongly peaked at the near resonant state due to the increase in ΔE and larger ΔN for other product states. Simulations of dispersed fluorescence spectra based on the McCaffery model provide less satisfactory agreement with experiment than those obtained using the energy gap model.

While the McCaffery model for collisional energy transfer can be used to explain the main trends in the experimental data, it may not be fully applicable to the present results. First, we cannot completely exclude the possibility that the initial VET process populates primarily the most near-resonant level and is then followed by partial rotational relaxation within OH $A^2\Sigma^+$ ($v' = 1$). Although such rotational relaxation is not observed in dispersed fluorescence spectra from the initially prepared OH $A^2\Sigma^+$ ($v' = 0, N'$) state, there remains the possibility of rotational relaxation within the product $v' = 1$ rotational manifold because of the smaller spacing between adjacent levels at lower N. In addition, the McCaffery model considers N_2 to be a structureless collision partner. This model has been successfully applied previously to vibration−rotation energy transfer of OH $A^2\Sigma^+$ in collisions with N_2, quasi-resonant vibration−rotation transfer of OH $X^2\Pi + N_2$,[24] and vibrational predissociation of OH−N_2.[27] Nevertheless, we point out for the sake of completeness that the OH $A^2\Sigma^+$ $v' = 0$ to 1 energy transfer process could result in rotational excitation of N_2; we also note that simultaneous vibrational excitation of OH and N_2 is not energetically open. Rotational excitation of N_2 could offset the change in rotational angular momentum of OH $A^2\Sigma^+$, possibly enabling additional product rotational levels (beyond the most near-resonant level) of OH $A^2\Sigma^+$ ($v' = 1$) to be populated by direct transfer from OH $A^2\Sigma^+$ ($v' = 0$).

In closing, we note that the state-to-state VET process in OH $A^2\Sigma^+$ from $v' = 0$ to 1 induced by collisions with N_2 described here was not observed with several other collision partners investigated, namely H_2, O_2, and CO_2 under similar experimental conditions. We suspect that the rates for VET with these partners are smaller than those for collisional quenching of OH $A^2\Sigma^+$ ($v' = 0$),[28,29] and thus the population transfer to OH $A^2\Sigma^+$ ($v' = 1$) is too small to be detected. This is consistent with observations at room temperature, where N_2 is known to be an unusual collision partner in being much more efficient in vibrational relaxation than quenching of OH $A^2\Sigma^+$.[7]

V. Conclusions

State-to-state vibrational energy transfer from OH $A^2\Sigma^+$ ($v' = 0$) to ($v' = 1$) induced by collisions with N_2 has been investigated at low collision energies. High rotational levels in OH $A^2\Sigma^+$ ($v' = 0$, $N' = 14-22$) are prepared by a multistep process involving laser excitation and collisional quenching. The OH $A^2\Sigma^+$ ($v' = 1$) products of VET are characterized through dispersed fluorescence spectra. Spectral simulations based on an assumed energy gap relationship are used to extract the OH $A^2\Sigma^+$ ($v' = 1$) product rotational distributions for each initially prepared level. The majority of the OH $A^2\Sigma^+$ ($v' = 1$, N') products are observed in the most near-resonant level of $v' = 1$ with population falling off rapidly in lower rotational levels. The near-resonant transfer involves a substantial change in rotational quantum number which increases as the initial rotational level of OH $A^2\Sigma^+$ ($v' = 0$) is decreased. The efficiency of transfer from the initially prepared OH $A^2\Sigma^+$ ($v' = 0$, N') level to $v' = 1$ is assessed by comparing the intensity of emission from $v' = 0$ and $v' = 1$. This analysis reveals that the fractional transfer changes by an order of magnitude over the range of initial rotational levels of OH $A^2\Sigma^+$ ($v' = 0$) investigated; a larger fraction is transferred to $v' = 1$ for higher initial rotational levels. The fractional transfer correlates inversely with the magnitude of the change in angular momentum between initial and final states, suggesting that angular momentum constraints control the efficiency of VET at low collision energies.

Acknowledgment. This research has been supported by the Office of Basic Energy Sciences of the Department of Energy. The authors thank Craig Murray, University of Bristol, for helpful discussions.

References and Notes

(1) Bailey, A. E.; Heard, D. E.; Paul, P. H.; Pilling, M. J. *J. Chem. Soc., Faraday Trans.* **1997**, *93*, 2915.
(2) Burris, J.; Butler, J. J.; McGee, T. J.; Heaps, W. S. *Chem. Phys.* **1988**, *124*, 251.
(3) Copeland, R. A.; Crosley, D. R. *J. Chem. Phys.* **1986**, *84*, 3099.
(4) Copeland, R. A.; Dyer, M. J.; Crosley, D. R. *J. Chem. Phys.* **1985**, *82*, 4022.
(5) Fairchild, P. W.; Smith, G. P.; Crosley, D. R. *J. Chem. Phys.* **1983**, *79*, 1795.
(6) German, K. R. *J. Chem. Phys.* **1976**, *64*, 4065.
(7) Steffens, K. L.; Crosley, D. R. *J. Chem. Phys.* **2000**, *112*, 9427.
(8) Dempsey, L. P.; Sechler, T. D.; Murray, C.; Lester, M. I.; Matsika, S. *J. Chem. Phys.* **2009**, *130*, 104307.
(9) Lester, M. I.; Loomis, R. A.; Schwartz, R. L.; Walch, S. P. *J. Phys. Chem. A* **1997**, *101*, 9195.
(10) Crosley, D. R.; Copeland, R. A. *Proc. SPIE-Int. Soc. Opt. Eng.* **1987**, *742*, 6.
(11) Joerg, A.; Meier, U.; Kienle, R.; Kohse-Hoeinghaus, K. *Appl. Phys. B: Laser Opt.* **1992**, *B55*, 305.
(12) Kienle, R.; Joerg, A.; Kohse-Hoeinghaus, K. *Appl. Phys. B: Laser Opt.* **1993**, *B56*, 249.
(13) Lengel, R. K.; Crosley, D. R. *Chem. Phys. Lett.* **1975**, *32*, 261.
(14) Crosley, D. R.; Smith, G. P. *Appl. Opt.* **1980**, *19*, 517.
(15) Smith, G. P.; Crosley, D. R. *Appl. Opt.* **1983**, *22*, 1428.
(16) Williams, L. R.; Crosley, D. R. *J. Chem. Phys.* **1996**, *104*, 6507.
(17) This observation is consistent with results of quantum scattering calculations for rotationally inelastic transitions of OH $A^2\Sigma^+$ in collisions with Ar at 300 K. See Table XII of Esposti, A. D.; Werner, H. J. *J. Chem. Phys.* **1990**, *93*, 3351.

(18) Schinke, R. *Photodissociation Dynamics*; Cambridge University Press: Cambridge, U.K., 1993.
(19) Dieke, G. H.; Crosswhite, H. M. *J. Quant. Spectrosc. Radiat. Transfer* **1962**, *2*, 97.
(20) Luque, J. Crosley, D. R. *LIFBASE: Database and Spectral Simulation Program*, V 1.6; SRI International Report No. MP 99−009; 1999.
(21) Clare, S.; McCaffery, A. J. *J. Phys. B: At., Mol. Opt. Phys.* **2000**, *33*, 1121.
(22) McCaffery, A. J. *J. Chem. Phys.* **1999**, *111*, 7697.
(23) McCaffery, A. J.; Marsh, R. J. *J. Phys. Chem. A* **2000**, *104*, 10442.
(24) McCaffery, A. J.; Marsh, R. J. *J. Phys. Chem. A* **2001**, *105*, 7135.
(25) McCaffery, A. J.; Osborne, M. A.; Marsh, R. J.; Lawrance, W. D.; Waclawik, E. R. *J. Chem. Phys.* **2004**, *121*, 169.
(26) Osborne, M. A.; McCaffery, A. J. *J. Chem. Phys.* **1994**, *101*, 5604.
(27) McCaffery, A. J.; Marsh, R. J. *J. Chem. Phys.* **2002**, *117*, 9275.
(28) Dempsey, L. P.; Murray, C.; Cleary, P. A.; Lester, M. I. *Phys. Chem. Chem. Phys.* **2008**, *10*, 1424.
(29) Dempsey, L. P.; Sechler, T. D.; Murray, C.; Lester, M. I. *J. Phys. Chem. A* **2009**, *113*, 6851–6858.

JP904978W